9th AUSTRALASIAN
FLUID MECHANICS CONFERENCE,
AUCKLAND, 8-12 DECEMBER 1986

Vortices and Unsteady flow in Turbulent Separation Bubbles

M. Kiya

Department of Mechanical Engineering, Hokkaido University, Sapporo, 060 Japan

ABSTRACT

This paper presents, for the leading-edge separation bubble of a two-dimensional blunt plate, the time-mean and r.m.s. velocities, the growth of the length scales of rolling-up vortices, the structure of large vortices in the reattaching zone of the separated shear layer, the unsteady flow associated with the motion of the large vortices, and the low-frequency unsteady structure. It is likely that these properties are similar to a wide range of separation bubbles behind salient edges.

1. INTRODUCTION

Flows at high Reynolds numbers with separation and reattachment (hereafter called as separation bubbles) appear in many engineering devices such as turbomachine blades, wings, pipe expansions and contractions, buildings during strong winds, etc. High heat-transfer rate in the reattaching zone of separated shear layers has been paid much attention (Hourigan et al.1985, Cooper et al. 1986). The r.m.s. surface pressure attains a maximum near the time-mean reattachment line (Kiya & Sasaki 1983a, Cherry et al. 1984).

Studies of vortex structures in the reattaching zone are still needed to elucidate mechanisms of the high heat-transfer rate and surface-pressure fluctuation, to manipulate the separation bubbles, and to develop numerical models for complex turbulent flows in general. Studies by Eaton & Johnston (1980), Kiya & Sasaki (1983a, 1985), Cherry et al. (1984), Troutt et al. (1984) and Ruderich & Fernholz (1986) demonstrate some properties of large vortices and unsteady flows in the separation bubbles. Manipulation of the separation bubbles is also tried by means of sound (Parker & Welsh 1983, Bhattacharjee et al. 1986), free-stream turbulence (Hillier & Cherry 1981, Kiya & Sasaki 1983b), periodically segmented separation edges (Gai & Sharma 1984, Kiya & Miyakoshi 1986).

In this paper the structure of large vortices and unsteady flow in a nominally two-dimensional separation bubble are discussed mainly based on results of Kiya & Sasaki (1983a, 1985). It is argued that general features of the vortices and the unsteady structure for this flow geometry are likely to be similar to those of a wide range of separation bubbles behind salient edges.

The geometry of flow and definition of symbols are illustrated in Fig. 1. The x-axis is taken in the longitudinal direction along a side (at the midspan) of a blunt plate of thickness 2H, the y-axis normal to the side and the z-axis normal to both x- and y-axes. The velocity components in the x-, y-, z-directions and the pressure are denoted by u, v, w, p which are divided into the time-mean components U, V, W(= 0), P and the fluctuating components u', v', w', p'. The velocity at infinity is U_∞. The distance from the separation edge to the time-mean reattachment line is written as x_R, which will be used as a representative length in the following discussion.

Unless otherwise stated, results presented in this paper are experimentally obtained in a wind tunnel at a Reynolds number of 23000. Measurements of the velocity fluctuations are made by single and X-wire probes and split-film probes operated by constant-temperature hot-wire anemometers. Surface-pressure fluctuations are measured by semiconductor strain-gauged pressure transducers. The reattachment length x_R is 10.1H.

2. TURBULENCE AND VORTEX STRUCTURES

2.1 Time-mean and turbulent velocities

The time-mean and r.m.s. longitudinal velocities are shown in Fig. 2. The separated shear layer is different from the two-dimensional plane mixing layer in that the former is bounded at its low-velocity side by a highly turbulent reverse flow. A part of fluid with turbulence is convected upstream from the reattaching zone and probably entrained into the rolling-up vortices in the separated shear layer. This is manifested by the fact that the maximum r.m.s. longitudinal velocity normalized by the actual velocity difference increases all the way from the separation line to the reattachment line. This is likely to be similar in a wide range of reattaching shear layers; for example, Ruderich & Fernholz (1986) obtain the same feature for a separation bubble behind a normal plate with a long splitter plate.

2.2 Length scales of vortices

The separated shear layer rolls up to form vortices as shown in Fig. 3. These photographs were taken in a water channel by a hydrogen bubble technique at Reynolds numbers of 580-680. A measure of the longitudinal length scale of the vortices can be obtained by the integral time scale of the autocorrelation coefficients of the velocity fluctuations u', v', w', q' (see the caption of Fig.4), multiplied by the free-stream velocity U_∞. As shown in Fig. 4, all of the four length scales measured at the outer edge of the shear layer are approximately the same. The linear increase of the length scales is a result of the successive vortex coalescence, so that their constancy downstream of the reattachment line indicates the absence of the vortex coalescence.

As is evident in Fig. 3, the vortices have a spanwise structure. The spanwise length scale of the vortices also grows linearly up to the reattachment line and remains constant downstream of it (Fig. 5). This trend is reasonable because vortices of larger cross section yields velocity fluctuations being more correlated in

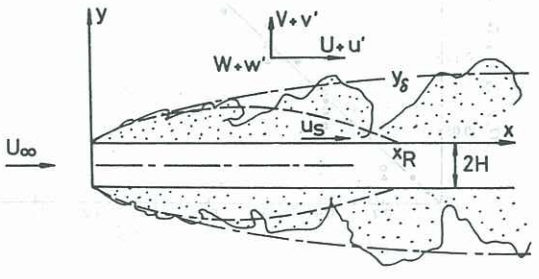

Fig. 1: Configuration of flow and definition of symbols.

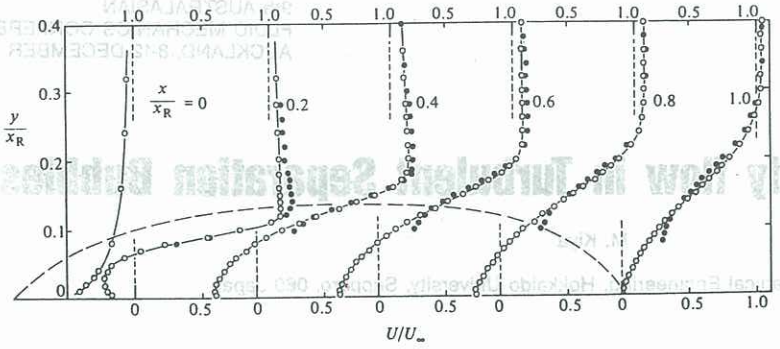

Fig. 2(a): Time-mean longitudinal velocity: o, split-film result; •, X-wire result; - - -, dividing streamline.

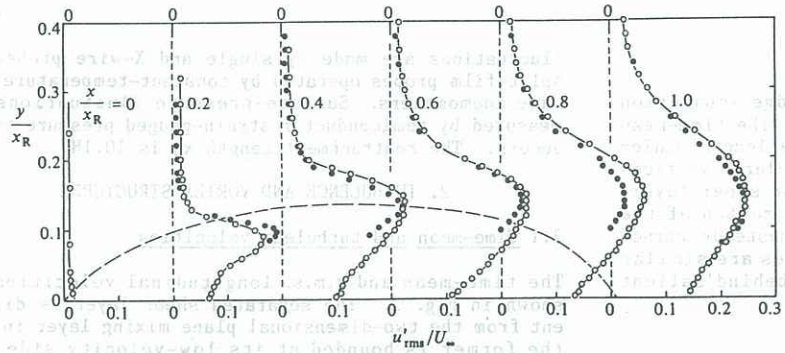

Fig. 2(b): R.m.s. longitudinal velocity: symbols as in Fig. 2(a).

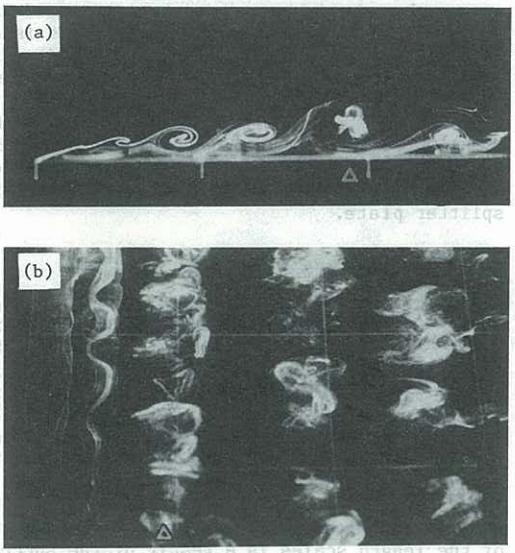

Fig. 3: Flow patterns in (a) the (x, y)-plane and (b) in the (x, z)-plane, Reynolds number being 680 and 580, respectively.

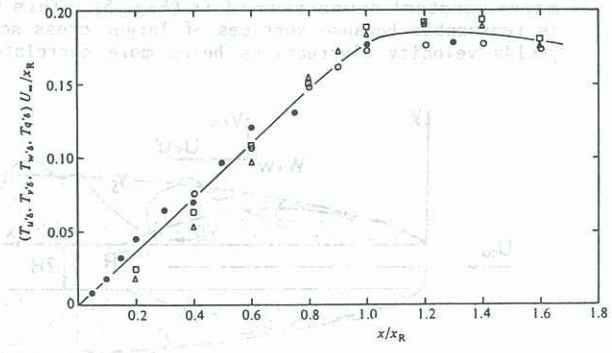

Fig. 4: Integral time scales at edge of shear layer: o, u'; Δ, v'; □, w'; •, q' (single hot-wire result).

the spanwise direction. It may be noted that, at the outer edge of the shear layer above the reattachment line, the spanwise length scale is about 2.6 times the longitudinal lenght scale which is the integral time scale multiplied by the local convection velocity.

2.3 Motion of vortices

The vortices are convected downstream with a velocity U_c which is equal to $0.55U_\infty$ at the centre of the shear layer above the reattachment line. The surface-pressure fluctuations yield the convection velocity $U_c = 0.50U_\infty$ at the reattachment line, which is close to the above value. The convection velocity obtained from the surface-pressure fluctuations slightly increases downstream. This increase is perhaps caused by the turbulent diffusion of vorticity (of the vortices), which reduces the circulation of the central part of the vortices and thus the velocity induced by image vortices.

The vortices are shed downstream from the separation bubble with a frequency of $(0.6\text{-}0.7)U_\infty/x_R$. This frequency is determined from the power spectrum of the surface pressure at the reattachment line (Fig. 6), that of u' at the edge of the shear layer, and the cross spectra of u' and v' at the centre and edge of the shear layer; all these spectra have a broad peak at the above frequency.

The shedding frequency and the convection velocity of the vortices yield an estimate of the longitudinal distance between two consecutive vortices downstream of

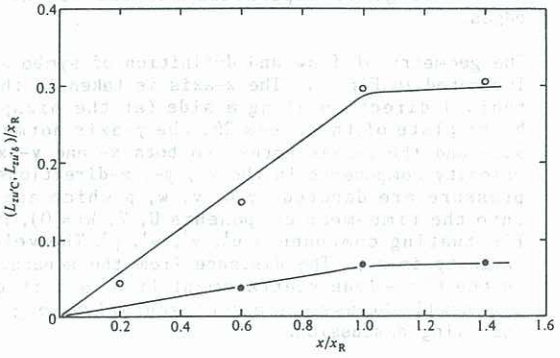

Fig. 5: Spanwise length scale of u' along centre (•) and at edge (o) of shear layer.

the reattachment line, which is $(0.8\text{–}0.9)x_R$. This seems to be consistent with the result of the flow visualization (Fig. 3).

2.4 Structure of large vortices

The motion of the vortices produces intense surface-pressure fluctuations near the reattachment line. A discrete-vortex simulation (Kiya et al. 1982) demonstrates that the fluctuating surface pressure is negative beneath a large vortex, attaining a definite minimum beneath its centre. This suggests that the structure of the vortices can be obtained by conditionally averaging the fluctuating velocities with respect to the time when the minima lower than a threshold level are detected.

Figures 7 and 8 show the conditionally averaged velocity fluctuations ($\langle u' \rangle$, $\langle v' \rangle$), ($\langle u' \rangle$, $\langle w' \rangle$) and high-frequency turbulent energy $\langle u_T'^2 \rangle$ in the space-time (y, t) and (z, t) domains. Here u_T' is the velocity fluctuation at frequencies of the order of the Kolmogorov frequency. A region where $\langle u_T'^2 \rangle$ attains a maximum is assumed to be a region of large vorticity, viz. the central part of the vortices.

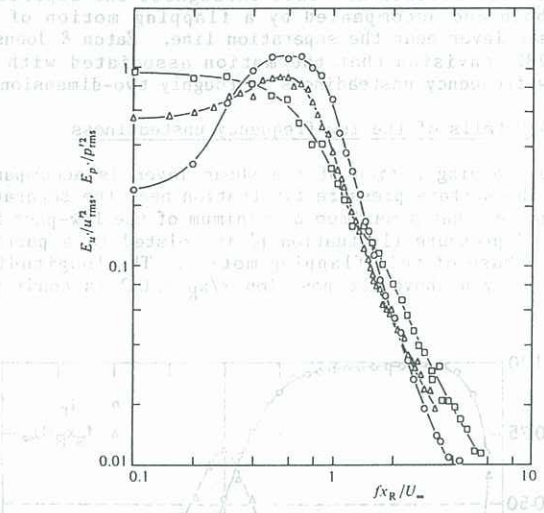

Fig. 6: Power spectra of longitudinal velocity at edge (o) and centre (□) of shear layer and surface-pressure fluctuation (Δ) at $x/x_R = 1.0$.

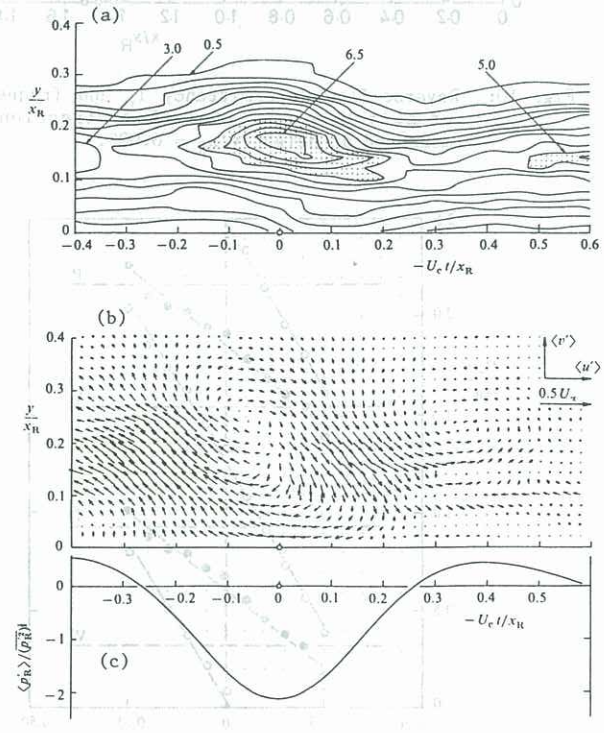

Fig. 7: Space-time (y, t) distributions of (a) high-frequency turbulent energy $\langle u_T'^2 \rangle$, fluctuating velocity vector ($\langle u' \rangle$, $\langle v' \rangle$) and (c) surface-pressure fluctuation $\langle p_R' \rangle$ at reattachment position.

A large system of flow rotating in the clockwise sense is seen in Fig. 7(b). Since $\langle u_T'^2 \rangle$ attains a maximum near the centre of the rotating system (Fig. 7(a)), this can be interpreted as a real vortex. The centre of the vortex seems to be located at a height $y/x_R = 0.18$.

The velocity vector ($\langle u' \rangle$, $\langle w' \rangle$) field in the space-time (z, t) domain near the edge of the shear layer ($y = 0.16x_R$) (Fig. 8(b)) shows a centre rotating in the clockwise sense at $(-z, -U_c t)/x_R = (0.28, -0.1)$ and another centre rotating in the counterclockwise sense approximately at (0.28, 0.25). The high-frequency energy $\langle u_T'^2 \rangle$ attains a maximum near the first centre (Fig. 8(c)). Moreover, from the symmetry, a centre rotating in the counterclockwise sense is expected at the image point (−0.28, −0.1) of the first centre. Accordingly these centres indicate a pair of counter-rotating vortices. On the other hand, the vector field near the centre ($y = 0.32x_R$) shows a sink-like point at $(-z, -U_c t)/x_R = (0, -0.25)$ and a source-like point at (0.1, 0.2), see Fig. 8(c).

The most economical interpretation of the space-time distributions of Figs. 7 and 8, although it may not be the only one, is that the vortices are hair-pin vortices as depicted in Fig. 9. The large vortices are the most dominant feature of turbulence in that they contribute to most of the Reynolds shearing stress and the surface-pressure fluctuation near the reattachment line. The Reynolds shearing stress is produced near the front and back edges of the vortices while the pro-

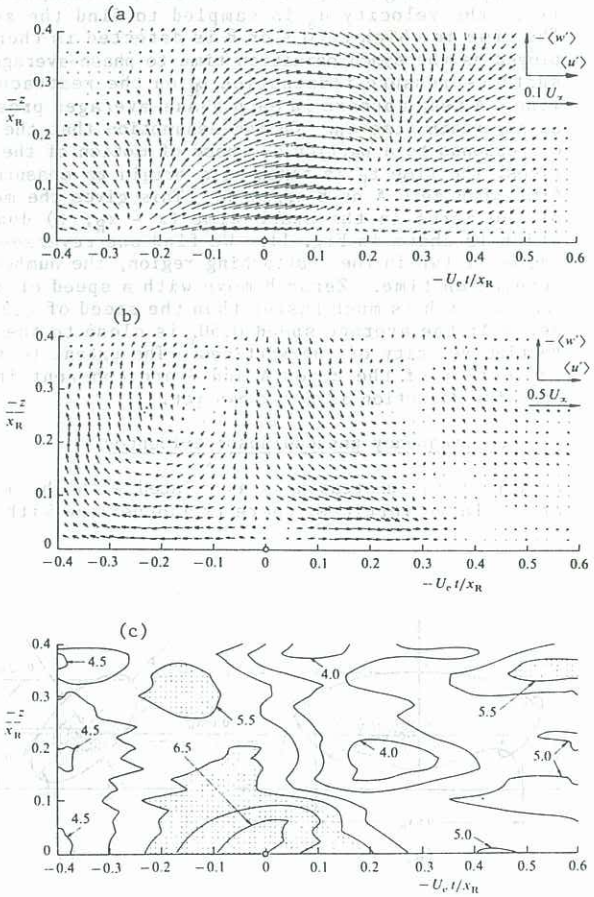

Fig. 8: Space-time (z, t) distribution of fluctuating velocity vector ($\langle u' \rangle$, $\langle w' \rangle$) at (a) edge and (b) centre of shear layer and (c) high-frequency energy $\langle u_T'^2 \rangle$ at centre of shear layer.

duction is negligible in the central part of the vortices.

3. UNSTEADY STRUCTURE OF SEPARATION BUBBLES

3.1 Reverse-flow intermittency and switching of the local-flow direction

The motion of the large vortices produces flow unsteadiness in the separation bubbles. Figure 10 shows the reverse-flow intermittency I_r measured near the surface (y/x_R = 0.005) as a function of the longitudinal distance. The time-mean reattachment position has been defined as a position where I_r = 0.5. A sharp decrease of I_r towards the separation edge suggests the formation of a small secondary separation bubble with the opposite direction of recirculation.

The unsteadiness can also be represented by the frequency f_s of switching of the local-flow direction, which is the number of switching from a forward to reverse flow (or from a reverse to forward flow) per unit time. This is included in Fig. 10. The frequency attains a maximum of $0.7U_\infty/x_R$ at the reattachment position, which is close to the vortex-shedding frequency.

3.2 Motion of reverse-flow regions

A reverse-flow region is defined as a region where the instantaneous longitudinal velocity u_s near the surface is negative; the velocity at the height y/x_R = 0.005 is chosen rather arbitrarily. This velocity is short-time averaged with an averaging time of about one-tenth of the vortex-shedding period. A boundary between a reverse-flow region and a forward-flow region is described by either $u_s = 0$, $du_s/dt < 0$, t being time, or $u_s = 0$, $du_s/dt > 0$, when u_s is measured at a fixed x position as a function of time; the former is denoted by zero A and the latter by zero B.

The motion of zeros A and B is obtained in the following way. At a given position x near the reattachment line, the velocity u_s is sampled to find the zeros. The time at which zero A or B is detected is then employed as the synchronization time to phase-average the surface-pressure fluctuation p_R' on the reattachment line. A peak appears in each phase-averaged pressure at a certain time t_p. On the assumption that the peak corresponds to a particular phase of motion of the vortices, the time t_p is taken as a origin to measure the time when zero A or B appears. This gives the motion of the zeros in the space-time ($x - x_R$, t) domain, which is shown in Fig. 11. We find one reverse-flow region or two in the reattaching region, the number depending on time. Zeros B move with a speed of about $0.7U_\infty$, which is much faster than the speed of $0.3U_\infty$ of zeros A; the average speed $0.5U_\infty$ is close to the convection velocity of the vortices. The extent to which the motion of the zeros A and B are coherent in the spanwise direction is not known yet.

3.3 Low-frequency unsteadiness; evidences

On top of the unsteadiness associated with the motion of the large vortices, there is another one with frequencies less than approximately $0.25U_\infty/x_R$, the central frequency being $0.12U_\infty/x_R$. It may be noted that this central frequency is much lower than the vortex-shedding frequency. The existence of this low-frequency unsteadiness is indicated by (i) a long tail of the auto correlation coefficient of u' near the centre of the shear layer at x/x_R = 0.2, (ii) energies in the low-frequency range of the surface-pressure spectrum at x/x_R = 0.2 (Fig. 12), (iii) a peak of the cross correlation of $0.25U_\infty/x_R$ Hz low-pass filtered surface-pressure fluctuations at two largely separated positions x/x_R = 0.2 and 1.0, and (iv) a spatial distribution of the cross correlation of the low-pass filtered longitudinal velocity fluctuations in the shear layer shortly down-stream of the separation line and the surface-pressure fluctuation at a fixed position x/x_R = 0.2.

From the features (iii) and (iv), the low-frequency unsteadiness is found to be of large scale in the sense that its effects are felt throughout the separation bubble and accompanied by a flapping motion of the shear layer near the separation line. Eaton & Johnston (1982) envision that the motion associated with the low-frequency unsteadiness is roughly two-dimensional.

3.4 Details of the low-frequency unsteadiness

The flapping motion of the shear layer is accompanied by the surface-pressure fluctuation near the separation edge, so that a maximum or minimum of the low-pass filtered pressure fluctuation p_l' is related to a particular phase of this flapping motion. The longitudinal velocity u above the position x/x_R = 0.2 is condition-

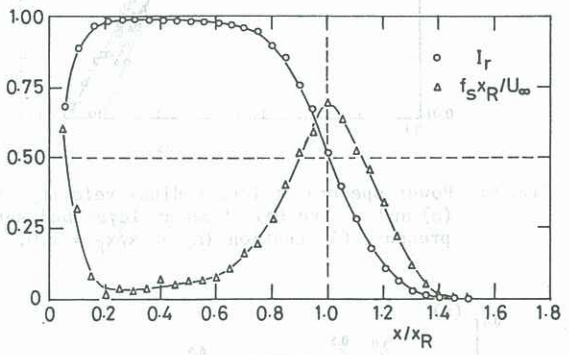

Fig. 10: Reverse-flow intermittency I_r and frequency of switching of local-flow direction f_s measured at height y/x_R = 0.005.

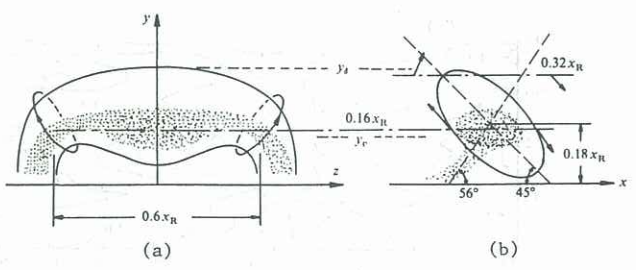

Fig. 9: Illustration of large vortices in reattaching zone: (a) structure in (y, z)-plane viewed from upstream side and (b) section in (x,y)-plane.

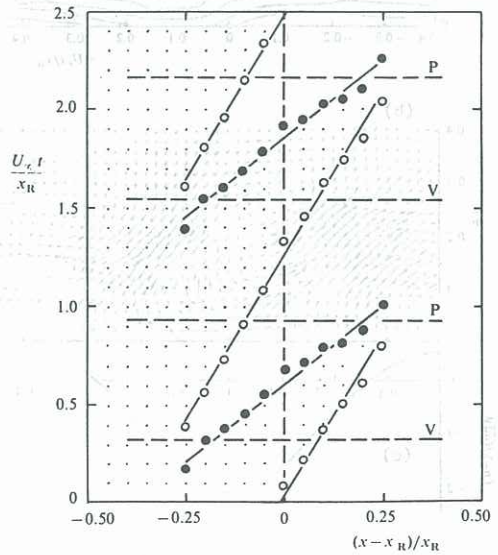

Fig. 11: Motion of zeros A and B of longitudinal velocity near surface in space-time ($x - x_R$, t) domain: o, zero A; •, zero B.

ally averaged at times when p_1' attains maxima greater than or minima lower than a threshold level. The result is shown in Fig. 13, which well establishes the existence of the flapping motion whose amplitude is of the order of $0.005x_R$. This rather small amplitude, however, is sufficient to yield a fluctuation of approximately $0.1U_\infty$ of the longitudinal velocity in the central part of the shear layer.

The low-frequency unsteadiness is also accompanied by a shrinkage and enlargement of the separation bubble, which respectively corresponds to maxima and minima of the $0.25U_\infty/x_R$ Hz low-pass filtered pressure fluctuation p_{R1}' at the reattachment position. The shrinkage and enlargement can be demonstrated by the motion of zeros of the low-pass filtered longitudinal velocity u_{s1} near the surface. There are two kinds of the zeros in the waveform of u_{s1} measured at a fixed position x; one is characterized by $u_{s1} = 0$ and $du_{s1}/dt < 0$ (denoted by zero A_1) and another by $u_{s1} = 0$ and $du_{s1}/dt > 0$ (denoted by zero B_1). In the same way as in §3.2, the motion of the zeros A_1 and B_1 is obtained with reference to the time when the maxima P_1 and minima V_1 of p_{R1}' appear.

The result is shown in Fig. 14. Zeros A_1 move upstream while zeros B_1 move downstream; the speed of A_1 and B_1 is approximately $0.1U_\infty$ and $0.2U_\infty$ in the middle of consecutive P_1 and V_1. In other words, the shrinkage is swifter than the enlargement. This has been suggested by Eaton & Johnston (1982).

The low-frequency unsteadiness produces a change in the strength of the large vortices. Figure 15 shows spectra of the surface-pressure fluctuation p_R' at the reattachment position, which are separately obtained in the shrunk and enlarged states. The spectrum for the shrunk state, for example, is calculated from the waveform during about a half of the central period of the low-frequency unsteadiness (centred around the time of the maxima P_1 of the low-pass filtered pressure p_{R1}'). In the same way the spectra for the enlarged state is calculated for the minima V_1. The spectra of Fig. 15 have a peak approximately at the frequency $0.6U_\infty/x_R$, which is close to the vortex-shedding frequency. The spectrum peak is much higher for P_1 than for V_1. This indicates that the large vortices shed during the shrunk state are stronger than those shed during the enlarged state because, the stronger the vortices, the greater is the surface-pressure fluctuation associated with the motion of the vortices.

An exact mechanism of the low-frequency unsteadiness is not known yet. Eaton & Johnston (1982) suggest that this is caused by an instantaneous imbalance between the entrainment (by the shear layer) from the recirculation zone and reinjection of fluid near the reattachment line. Moreover the somewhat fair periodicity of the low-frequency unsteadiness (see Fig. 14) indicates a feedback of disturbances from the reattachment zone to the shear layer near the separation edge (Rockwell 1983).

4. CONCLUDING REMARKS

This paper has discussed, for the leading-edge separation bubble of a two-dimensional blunt plate, the time-mean and r.m.s. velocities, the growth of the length scales of the rolling-up vortices, the structure of the large vortices near the reattachment line, their dynamical significance, the unsteady flow associated with the motion of the large vortices, and the structure of the low-frequency unsteadiness. It is likely that these properties are similar in a wide variety of sepa-

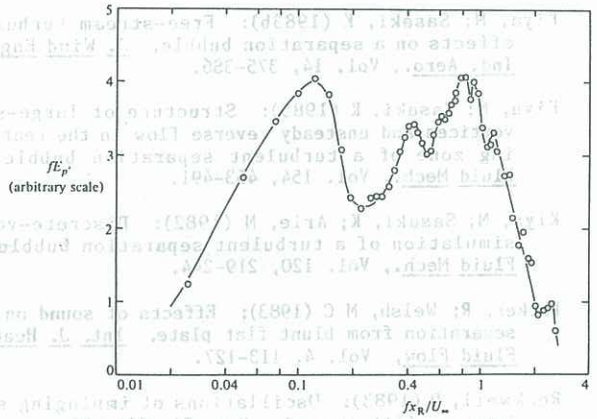

Fig. 12: Surface-pressure spectrum at section $x/x_R = 0.2$.

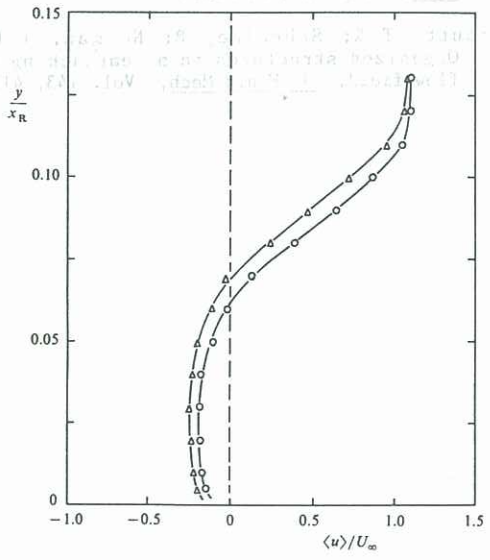

Fig. 13: Longitudinal-velocity profile conditionally averaged at time when surface pressure at $x/x_R = 0.2$ attains maxima (Δ) and minima (o).

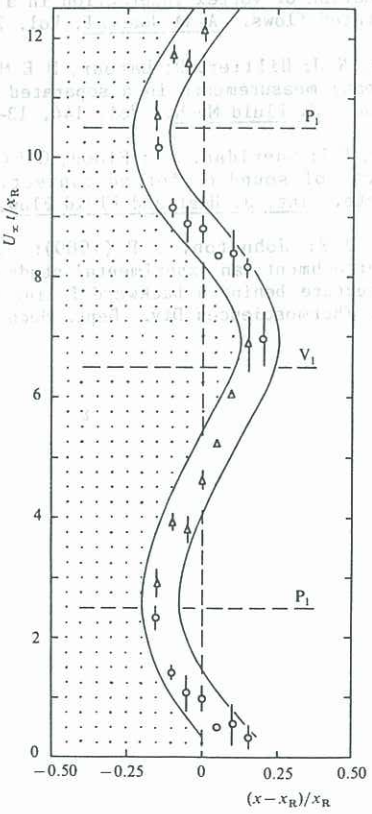

Fig. 14: Motion of zeros A_1 (Δ) and B_1 (o) of longitudinal velocity near surface in space-time ($x - x_R$) domain.

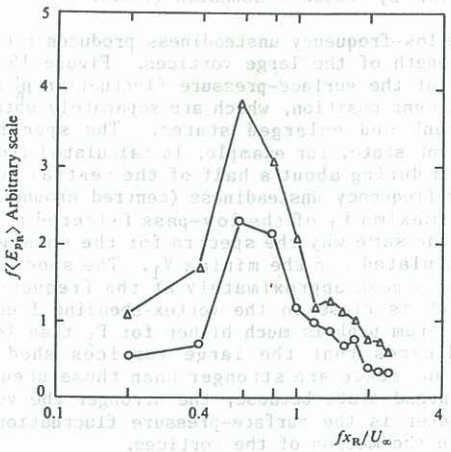

Fig. 15: Pressure spectra for enlarged (o) and shrunk (Δ) states of separation bubble due to low-frequency unsteadiness.

ration bubbles formed at salient edges. For example, the low-frequency unsteadiness is also found for separation bubbles behind a normal plate with a long splitter plate (Cherry et al. 1984), behind a downward-facing step (Eaton & Johnston 1982) and at the leading edge of a blunt circular cylinder (Kiya & Nozawa 1986), and even for the blunt-plate separation bubble with a turbulent free stream (Cherry et al. 1984). Finally it should be remarked that the surface-pressure fluctuation is successfully uesd as a conditioning signal to obtain the structure of the large vortices and that of the unsteady flow.

REFERENCES

Bhattacharjee, S; Scheelke, B; Troutt, T R (1986): Modfication of vortex interaction in a reattaching separated flows. AIAA Journal, Vol. 24, 623-629.

Cherry, N J; Hillier, R; Latour, M E M P (1984): Unsteady measurements in a separated and reattaching flow. J. Fluid Mech., Vol. 144, 13-46.

Cooper, P I; Sheridan, J C; Flood, G J (1986): The effects of sound on forced convection over a flat plate. Int. J. Heat and Fluid Flow, Vol. 7, 61-68.

Eaton, J K; Johnston, J P (1980): Turbulent flow reattachment: an experimental study of the flow and structure behind a backward facing step. Rep. MD-39, Thermosciences Div., Dept. Mech. Eng., Stanford University.

Eaton, J K; Johnston, J P (1982): Low-frequency unsteadiness of a reattaching shear layer. Turbulent Shear Flows 3 (ed. L J S Bradbury; F Durst; B E Launder; F W Schmidt; J W Whitelaw), 162-170.

Gai, S L; Sharma, S D (1984): Subsonic turbulent flow over a rearward facing segmented step. Phys. Fluids, Vol .27, 544-546.

Hillier, R; Cherry, N J (1981): The effects of stream turbulence on separation bubbles. J. Wind Eng. and Ind. Aero., Vol. 8, 49-58.

Hourigan, K; Welsh, M C; Welch, L W (1985): Augmented forced convection around a heated flat plate. 23rd AIChE/ASME National Heat Transfer Conference, Denver, Colorado, August, 4-7, 1985, 1-9.

Kiya, M; Miyakoshi, M (1986): Manipulation of separated and reattaching flow by spanwise segmentation. Trans. JSME (to be published).

Kiya, M; Nozawa, T (1987): Turbulence structure in the leading-edge separation zone of a blunt circular cylinder. Trans. JSME (to be published).

Kiya, M; Sasaki, K (1983a): Structure of a turbulent separation bubble. J. Fluid Mech., Vol. 137, 83-113.

Kiya, M; Sasaki, K (1983b): Free-stream turbulence effects on a separation bubble. J. Wind Eng. and Ind. Aero., Vol. 14, 375-386.

Kiya, M; Sasaki, K (1985): Structure of large-scale vortices and unsteady reverse flow in the reattaching zone of a turbulent separation bubble. J. Fluid Mech., Vol. 154, 463-491.

Kiya, M; Sasaki, K; Arie, M (1982): Discrete-vortex simulation of a turbulent separation bubble. J. Fluid Mech., Vol. 120, 219-244.

Parker, R; Welsh, M C (1983): Effects of sound on flow separation from blunt flat plate. Int. J. Heat and Fluid Flow, Vol. 4, 113-127.

Rockwell, D (1983): Oscillations of impinging shear layers. AIAA Journal, Vol. 21, 645-664.

Ruderich, R; Fernholz, H H (1986): An experimental investigation of a turbulent shear flow with separation, reverse flow, and reattachment. J. Fluid Mech, Vol. 163, 283-322.

Troutt, T R; Scheelke, B; Norman, T R (1984): Organized structures in a reattaching separated flow field. J. Fluid Mech, Vol. 143, 413-427.